ELSEVIER

Polymer 44 (2003) 3107–3116

polymer

www.elsevier.com/locate/polymer

Structural changes in non-isothermal crystallization process of melt-cooled polyoxymethylene. [I] Detection of infrared bands characteristic of folded and extended chain crystal morphologies and extraction of a lamellar stacking model

Hisakatsu Hama, Kohji Tashiro*

Department of Macromolecular Science, Graduate School of Science, Osaka University, Toyonaka, 1-1 Machikaneyama-cho, Toyonaka Osaka 560-0043, Japan

Received 6 November 2002; received in revised form 17 January 2003; accepted 20 February 2003

Abstract

Structural change in the crystallization process of polyoxymethylene (POM) cooled from the molten state has been investigated by the measurements of infrared spectra and small-angle (SAXS) and wide-angle X-ray scatterings (WAXS). When the melt was cooled slowly, the infrared bands characteristic of a folded chain crystal (FCC) were observed to appear around 156 °C. Below 140 °C, the infrared bands intrinsic of an extended chain crystal (ECC) were detected to increase in intensity. In the SAXS measurement, the peak (L_1) corresponding to a stacked lamellar structure with the long period of ca. 14 nm was found to grow in parallel to the growth of infrared FCC bands. In the temperature region of the observation of infrared ECC bands, the new peak (L_2) of long period of ca. 7 nm was found to appear and the intensity exchange occurred between the L_1 and L_2 peaks, that is, with decreasing temperature the L_2 peak increased the intensity and its height became comparable to the L_1 peak height. By combining all these experimental data, a model to illustrate the formation process of lamellar stacking structure has been presented. After the appearance of stacked lamellar structure of 14 nm long period from the melt, new lamellae are created in between the already existing lamellae and the long period changes to the half value, 7 nm. Some of molecular chain stems in a lamella are speculated to pass through the adjacent lamellae to form a bundle of fully extended taut tie chains, which are considered to be observed as the infrared bands characteristic of ECC morphology. Although the POM samples used in this experiment may contain small amount of low-molecular-weight macrocyclic component, it was not plausible judging from the various experimental data to assign the secondarily observed 7 nm SAXS peak to the repeating period originating from the stacked structure of macrocyclic compounds.

Keywords: Polyoxymethylene; Crystallization process; Infrared spectra

1. Introduction

In order to control the so-called higher-order structure of polymers and to develop new materials with excellent physical properties, we need to clarify the formation process of the higher-order structure from the various points of view. Enormous numbers of reports have been published so far about the crystallization behaviors of various kinds of multi-purpose polymer such as polyethylene, *isotactic* polypropylene, etc. As one of the typical engineering plastics we know polyoxymethylene (POM), which is important both industrially and scientifically. The crystallization of POM has been investigated extensively from various points of view [1–25]. But, as to the time-dependent structural evolution or even the static structural change in the crystallization process from the molten state only limited number of papers have been published so far [12–25]. One of the reasons may come from the characteristic features of POM sample. For example, thermal decomposition occurs relatively easily when the POM sample is melted and kept at high temperature for a while. The sample generates many bubbles, making the small-angle X-ray scattering (SAXS) measurement quite difficult. One idea to escape from this problem is to employ a copolymer of trioxane with a small amount of other

* Corresponding author. Tel.: +81-6-6850-5455; fax: +81-6-6850-5455.
E-mail address: ktashiro@chem.sci.osaka-u.ac.jp (K. Tashiro).

0032-3861/03/$ - see front matter © 2003 Elsevier Science Ltd. All rights reserved.
doi:10.1016/S0032-3861(03)00207-6

monomer such as ethylene oxide. Of course, strictly speaking, the crystallization temperature as well as the melting temperature might be modified more or less depending on the content of this comonomer, but the crystallization behavior is essentially the same with that of the original POM homopolymer, as judged from the various experimental results collected for the various types of POM copolymer.

Another point to be noticed is a complicated morphology of POM sample. As the typical crystalline morphologies of POM we know an extended chain crystal (ECC) and a folded chain crystal (FCC). FCC of POM was found out from the dilute solution in an early stage of discovery of polymer single crystals [26–28]. ECC of POM was found as a product of cation polymerization of trioxane [29]. Shish-kebab structure or a hybrid structure of ECC and FCC was also observed for the oriented overgrowth crystallization of the molten POM on the needle-shaped POM single crystal [30]. In this way, the morphology of POM changes in various manners depending on the sample preparation condition. How can we study these morphologies of POM from the molecular level? For example, Shimomura and Iguchi [31] discovered a remarkable difference in the infrared spectra between ECC and FCC. Fig. 1 shows a series of infrared spectra taken for the POM samples prepared under various crystallization conditions. The spectrum (a) is for the single crystal mat prepared in hexafluoro-isopropanol (HFIP) solution, which consists mainly of FCC and gives several infrared bands intrinsic of FCC morphology. The spectrum (d) was measured for the whisker obtained from the cationic polymerization of trioxane, having a typical ECC morphology. Intense A_2 band at ca. 900 cm^{-1} is characteristic of ECC state. The spectrum (b) is about the film cast from HFIP solution with the ECC band as a shoulder. The sample (c) was prepared by

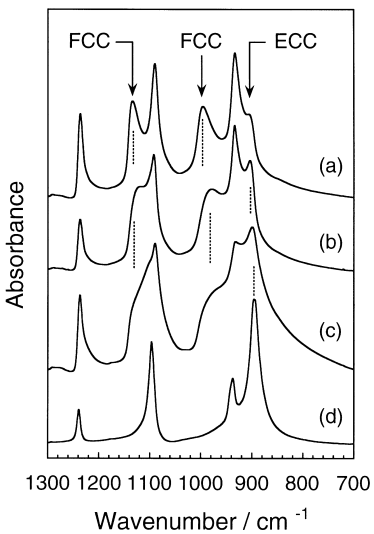

Fig. 1. Infrared spectra of POM samples prepared under the various conditions. (a) Solution-grown lamellar mat, (b) film cast from HFIP solution, (c) film cooled from the melt, and (d) whisker.

cooling the melt and exhibits the ECC bands more clearly, allowing us to speculate that the POM sample crystallized from the melt is a mixture of ECC and FCC in a complicated manner. Kobayashi et al. interpreted a remarkable difference in the infrared spectra by introducing dipole–dipole interactions in the crystallite [32]. The vibrational frequency of an A_2 mode is dependent on the total summation of these interactions over a crystallite or on the shape of the crystallite. That is to say, a remarkable difference in spectral profile observed in Fig. 1 is considered to come from the difference in crystallite morphology. In other words, the crystallite morphology may be estimated from the profile of the observed infrared spectra. In the present study, we will investigate the structural change in the crystallization process of POM by tracing the infrared spectral changes, which should reflect any change in crystallite morphology.

In order to make the thus obtained morphological information more concrete, the SAXS and WAXS measurements are also useful. In particular, the SAXS data may tell us the aggregation state of crystalline lamellae. In the present paper our focus is mainly on the analysis of infrared spectral data as mentioned above, but the SAXS and WAXS data are compared with the infrared spectral data and a plausible model will be proposed about the formation of lamellar stacking structure in the crystallization process of POM. More detailed analysis of SAXS and WAXS data will be reported separately.

There might be two experimental ways to investigate the crystallization from the melt. One way is to change the temperature of the sample continuously from the melt, during which the X-ray diffraction and infrared spectra are measured as a function of temperature. Another way is to change the temperature suddenly from above the melting point to below the crystallization point or the so-called temperature jump and to collect the data during the isothermal crystallization process as a function of time. The latter is more ideal for the purpose to trace the structural evolution at a constant temperature in association with the nucleation and growth of crystallites. But, as the first trial of our above-mentioned strategy, we will report here the experimental data collected in the slow cooling process from the melt or in the non-isothermal crystallization process. The results on isothermal crystallization will be reported elsewhere.

2. Experimental

2.1. Samples

In order to avoid thermal degradation as much as possible, a copolymer of trioxane with small content of ethylene oxide (ca. 2.2 wt%, Duracon M90, Polyplastics Co. Ltd, Japan) was used as a sample. The M_w was ca. 69300 g/mol and M_w/M_n ca. 2.3. As judged from the DSC, X-ray diffraction and IR spectral measurements, the

crystallization behavior was essentially the same with that of the homopolymer, although the melting and crystallization points were slightly different from those of the homopolymer.

2.2. Measurements

2.2.1. Thermal analysis

DSC thermograms were measured by a Perkin–Elmer Pyris 1 at heating and cooling rates of 0.5 °C/min to check the thermal behavior of the sample.

2.2.2. FTIR measurement

Infrared spectra were measured by using a Bio Rad FTS-60A/896 Fourier-transform infrared spectrometer at a resolution power 2 cm^{-1}. The sample was sandwiched between a pair of KBr plates and set into an optical cell equipped with a heater. The heating and cooling rates were about 0.3 °C/min, during which each spectrum was measured for 20 s at an interval of 200 s.

2.2.3. SAXS and WAXS measurements

Temperature dependences of SAXS and WAXS were measured by using synchrotron radiation as an X-ray source at beam lines BL10C and BL15A, respectively, in Photon Factory of High-Energy Accelerator Research Organization in Tsukuba, Japan. The wavelength of incident X-ray beam was 0.149 nm in both of BL10C and BL15A. The temperature was changed step by step from 205 °C to room temperature. The X-ray exposure time was 15 s in both the SAXS and WAXS measurements. The detector was a PSPC (position sensitive proportional counter) for both of the measurements. In the analysis of SAXS and WAXS data, the correction of background and fluctuation of beam intensity was made and the scattering intensity $I(q)$ was transformed to $I(q)q^2$ for the correction of Lorentz factor, where q was a photon vector and was defined as $q = (4\pi \times \sin\theta)/\lambda$, where λ was a wavelength of incident X-ray beam and 2θ was a scattering angle.

3. Results and discussion

3.1. Determination of optimal melting conditions

As mentioned in Section 1, POM samples are easily damaged when they are heated above the melting point (about 160 °C) for a long time. This occurs even when an inert gas is flowed around the sample. Keeping the sample above the melting point for only a short time seems good to avoid the oxidation of the sample. But such a short melting cannot erase perfectly the previous history of the sample to be used in the next experiment. A small amount of lamella residue, for example, might accelerate the crystallization from the melt. Therefore, we need to find the optimal condition to perfectly melt the sample without almost any thermal degradation and to erase any sample history.

The POM sample packed in a DSC pan was kept at a preset temperature above the melting point for a predetermined time (5–30 min) and cooled quickly to 140 °C, at which the DSC thermogram was measured as a function of time. The 140 °C was chosen as a representative crystallization temperature. The time dependence of crystallinity was estimated by integrating the DSC thermogram at a constant interval of time. The result is shown in Fig. 2. When the sample was melted at 200 °C for 25–30 min, the crystallization was relatively slow and reproducible. But, when the sample was melted for a shorter time of 5–10 min at 200 °C, the crystallization occurred faster, indicating an insufficient erasing of preexisting lamellae, which worked as a nucleation agent and accelerated the crystallization rate. On the other hand, when the sample was melted at 205 °C, the heating for 5–15 min gave almost the same result with the case of heating for 25–30 min at 200 °C. But a longer heating at 205 °C caused a thermal decomposition significantly and the crystallization rate was higher possibly because of the reduction of molecular weight due to thermal decomposition. As shown in Fig. 3, the melting behavior of these samples was also investigated. The melting of the sample treated at 200 °C for 20–30 min gave a reproducible endothermic peak around 158 °C. But this peak was observed at higher temperature due to an influence of residual lamellae when the treatment time was shorter. The sample treated at 205 °C for a short time melted at a similar temperature with the sample treated at 200 °C for a long time. Longer treatment at 205 °C gave a remarkable shift of melting peak to a higher temperature side, reflecting a thermal decomposition although the reason of high temperature shift of the melting point was not clear. From these data of Figs. 2 and 3, we concluded that the heating at 205 °C for 5 min might be the best condition for getting almost perfectly molten sample without any memorial effect of residual lamellae and almost any detectable thermal decomposition. The infrared and X-ray diffraction

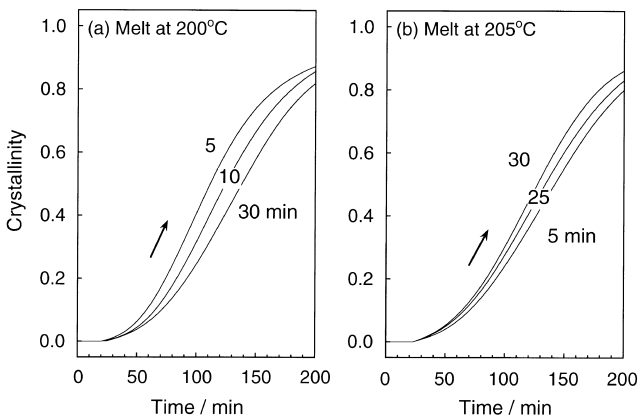

Fig. 2. Time dependence of crystallinity estimated from the DSC thermogram in the isothermal crystallization at 140 °C after holding a POM sample at 200 or 205 °C for different hold time shown in figures.

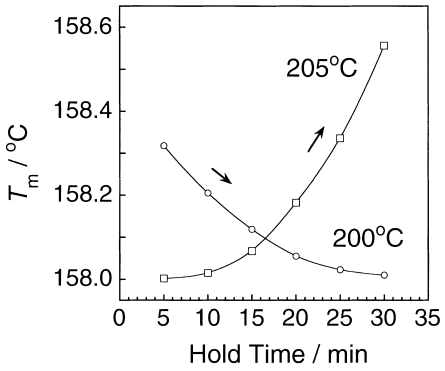

Fig. 3. Comparison of melting behavior between the POM samples which were melted at 200 or 205 °C for different hold time and then quenched to 140 °C.

measurements were started in the cooling process after the sample was kept under the thus-determined condition, as will be mentioned in the following sections. The equilibrium melting temperature was estimated to be about 187 °C by plotting the observed melting point against the crystallization temperature (Hoffman–Weeks plot) [33], which seems reasonable compared with the homopolymer's value (184 ± 2 [34], 186.4 [35], 189.7 ± 0.7 [36] or 189.2 °C [37])

3.2. Temperature dependence of IR spectra

Temperature dependence of infrared spectra was measured in both the cooling process from the melt and the second heating process as shown in Figs. 4 and 5, respectively. In these figures, the spectra at 180 and 200 °C are of the molten state. As the temperature was decreased (Fig. 4), the bands characteristic of FCC were detected at

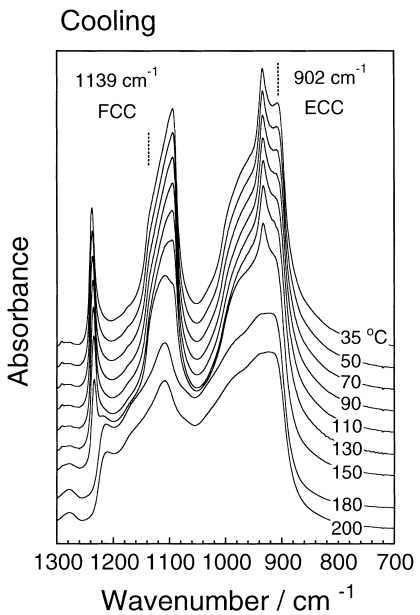

Fig. 4. Temperature dependence of infrared spectra of POM taken in the cooling process from the melt.

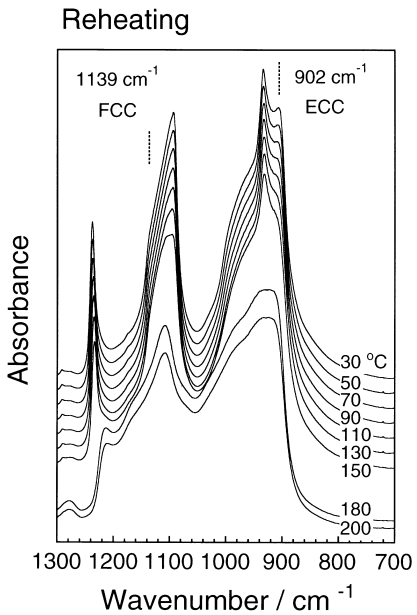

Fig. 5. Temperature dependence of infrared spectra of POM taken in the heating process.

first around 156 °C. The band at 902 cm^{-1} is due to ECC and began to appear around 140 °C. When the sample was heated again (Fig. 5), the ECC band decreased in intensity at first and then the FCC bands decreased their intensity at about 165 °C (Fig. 8).

These spectra were analyzed quantitatively to estimate the temperature dependence of the ECC and FCC band intensity. Many bands were overlapped together, making the evaluation of intensity change difficult. Then the analysis was carried out in three ways. One was a separation of band components by assuming the band profiles. But this method was not suitable for the spectra of POM because the spectra of the melt or amorphous phase are broad and contain too many bands. Next a self-deconvolution method was tried to get sharper profiles by assuming several types of window function intrinsic of the spectrometer [38]. But this method was also hard to uniquely estimate the intensity of individual peak due to the same reason with above. As the third method, the spectra were differentiated twice with respect to wavenumber in order to get the second-derivatives of the spectral profiles. Fig. 6 shows a comparison between the original spectra and their second derivatives. We can separate the sharp bands of the crystalline phase clearly from the broad bands of the amorphous region. The intensity I estimated for these second-derivatives curves is not directly proportional to the intensity of the original band but is affected by the half width.

I(second-derivatives) ∝ (peak height of the band)/

(half-width)^2

Therefore, the intensity is underestimated than the true value due to the effect of finite band width. As long as the

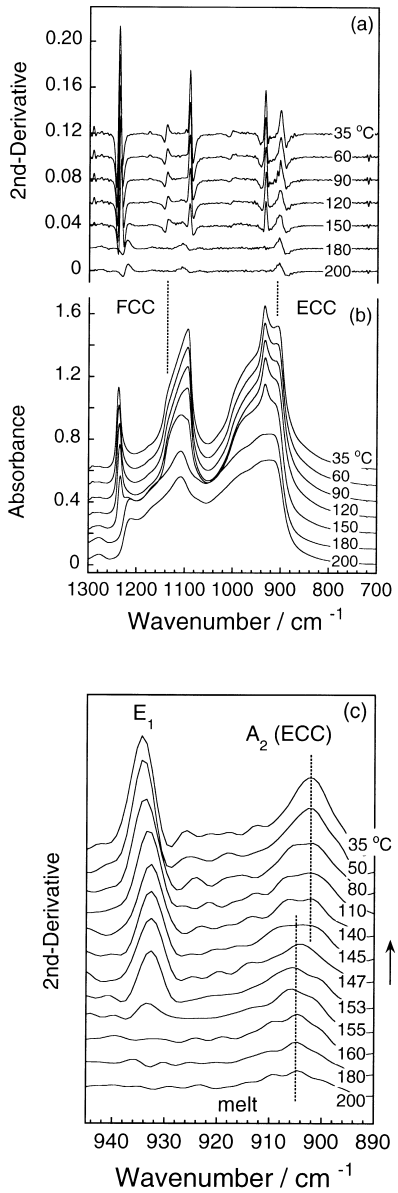

Fig. 6. Temperature dependence of (a) the second derivatives curve and (b) the original infrared spectra of POM (see Fig. 4). In (c), the curves of (a) are zoomed up to clarify the spectral changes in the frequency region of 890–940 cm^{-1}.

band width is not very largely changed, the intensity of the second-derivatives curve may be assumed to be proportional to the intensity of the original band. In the present paper, therefore, as the first approximation, the height of the second-derivatives is used to represent the intensity of the original infrared band. In Figs. 7 and 8 is plotted the thus evaluated intensity against temperature for both the ECC (902 cm^{-1}) and FCC (1139 cm^{-1}) bands in comparison with the DSC thermogram. In the cooling process (Fig. 7), the FCC band started to appear at ca. 156 °C and increased in intensity quite sharply. The ECC band started to appear at lower temperature than the FCC band around 140 °C and grew up slowly with decreasing temperature. In the heating process (Fig. 8), the ECC band intensity decreased gradually

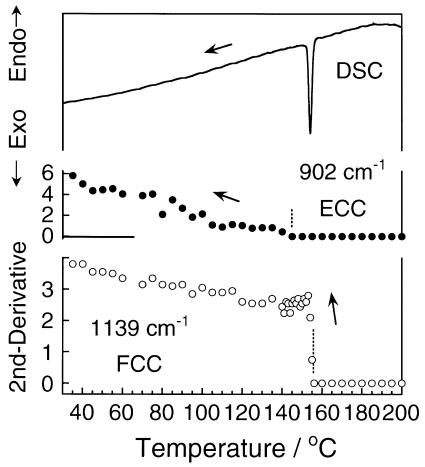

Fig. 7. Temperature dependence of the band intensity estimated from the second derivatives curves (Fig. 6) in comparison with the DSC thermogram (cooling process).

with increasing temperature and disappeared around 130 °C. The FCC band could be observed still in this temperature region and disappeared steeply around 165 °C. Sharp DSC peak corresponds to the temperature of appearance and disappearance of the FCC band. The gradual change in ECC band intensity may correspond to the broad background detected in the DSC thermogram, through not very clear.

In this way the infrared bands intrinsic of ECC and FCC were found to behave in a different manner. The ECC band appeared and disappeared in rather broad and lower temperature region compared with the FCC bands. This seems curious when we imagine the typical morphology of ECC and FCC. The ECC may be assumed as an almost perfect crystal consisting of fully extended chains and the FCC is an imperfect crystal of short stems with folded parts on wide surfaces. Therefore the melting (and crystallization) temperature should be much higher for ECC than FCC. In fact, as shown in Figs. 9 and 10, the infrared bands of POM whisker disappeared at ca. 190 °C, much higher than the

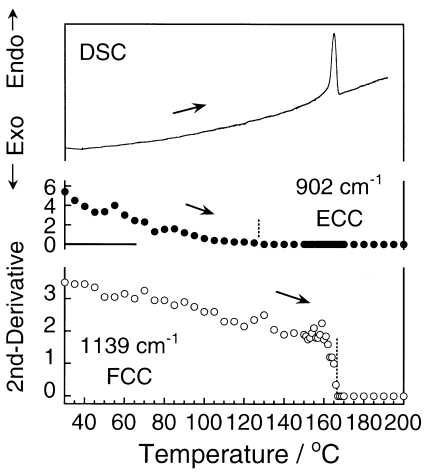

Fig. 8. Temperature dependence of the band intensity estimated from the second derivatives curves in comparison with DSC thermogram (heating process).

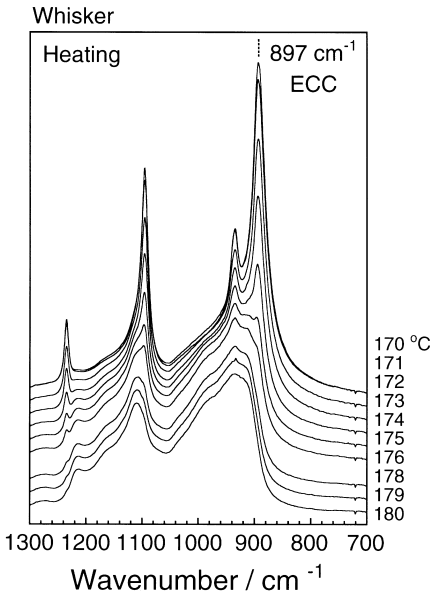

Fig. 9. Temperature dependence of infrared spectra of POM whisker measured in the heating process.

melting of the ECC bands shown in Fig. 8. Therefore the ECC morphology found in Figs. 4 and 5 should have much smaller dimension than the whisker of μm size. According to the theory [32], the vibrational frequency ν is determined as the product of oscillation strength of the mode and the geometrical factor. When the shape of a crystallite is assumed to be a cylinder with radius R and height H, the vibrational frequency is a function of ratio R/H. Since a whisker has a ratio R/H of almost zero value because the cylindrical height H is overwhelmingly long compared with the radius R, the vibrational frequency should be observed at the same position with that of a single crystal. The ECC band was observed at 902 cm^{-1} in the present crystallization experiment, which is close to the vibrational frequency 897 cm^{-1} observed for a whisker sample. Therefore the crystalline region giving the ECC band is speculated to have almost the same R/H ratio with that of whisker, but the absolute values of R and H may be much smaller than those of the whisker. Because of this small size, the 'ECC-like' morphology is considered to give lower melting point compared with that of a whisker (Fig. 10).

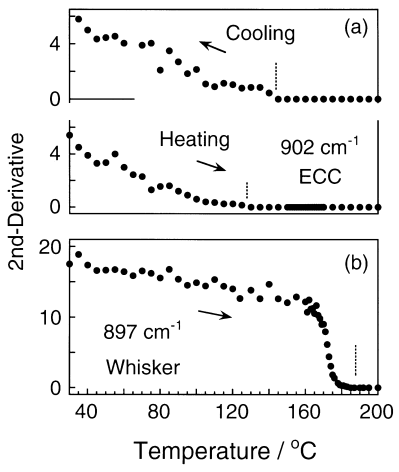

Fig. 10. Temperature dependence of the ECC band intensity estimated from the second derivatives curves. (a) Melt-cooled POM sample and (b) POM whisker.

3.3. Temperature dependence of SAXS and WAXS

Temperature dependence of SAXS profile taken in the cooling process from the melt is shown in Fig. 11. Around 155 °C a peak L_1 started to appear and increased in intensity with slight shift of the peak position toward higher q side. In the temperature region of 140 °C another peak L_2 started to appear and increased in intensity gradually. In parallel the intensity of the L_1 peak decreased and became comparable to that of the L_2 peak at room temperature. The positions of L_1 and L_2 peaks correspond to the long periods of 14 and 7 nm at 30 °C, respectively, and the L_1 is almost twice the L_2. Therefore it might be assumed that the L_2 is the second order peak of L_1. But, judging from the quite different temperature behavior of these two peaks, the L_2 peak cannot be assigned to the second order peak of the L_1 peak. That is to say, some complicated structural change is speculated to occur in the crystallization process.

Another important point to be noticed here is that the temperature region to observe the SAXS L_1 peak is almost equal to the region to observe the infrared FCC bands. The same situation can be seen also between the SAXS L_2 peak and the infrared ECC bands. In a separate paper we will report the time dependence of SAXS profile collected in the isothermal crystallization experiment, in which the L_1 peak appeared in an early stage of crystallization and the L_2 peak appeared in much later timing. The time-resolved infrared spectral measurement was also made in the isothermal crystallization experiment, from which the

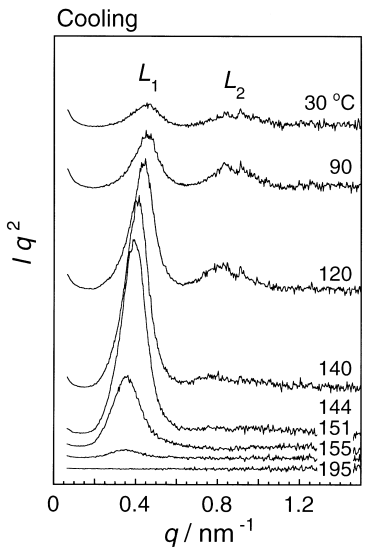

Fig. 11. Temperature dependence of SAXS profile of POM sample measured in the cooling process.

good correspondence of the detection timing was observed between the SAXS and infrared data; that is, the L_1 peak to the FCC band and the L_2 peak to the ECC band. All of these experimental data support definitely our speculation that the L_1 and L_2 peaks come from the different origins.

Assignment of SAXS L_1 and L_2 peaks had been an unsolved problem for a long time for various polymer samples [23]. In some cases, the L_1 and L_2 peaks are assigned to the first-order and second-order peaks originating from a lamellar stacking structure, even when the ratio of long periods evaluated from these two peaks is not exactly 2 but 2.3, for example. This non-integer ratio has been considered to come from the stacking disorder of amorphous thickness or crystalline lamellar thickness as being interpreted on the basis of Hosemann's second kind of paracrystalline theory [39–41]. Another case is that the L_1 and L_2 may come from the different origins. The present POM sample is considered to be of this second case. In an extreme case, the L_1 might be assigned to the stacked lamellar structure of FCC morphology and the L_2 to the stacking structure of ECC because we know a good correspondence between the SAXS peaks and infrared spectral data: the L_1 to FCC bands and the L_2 to ECC bands. Fig. 12 illustrates the several types of structural models. Model (a) shows a coexistence of two kinds of lamellar stacking structure in the sample: an aggregation of FCC-type lamellae with the long period L_1 and an aggregation of short chain stems with the period L_2. By taking into account the good correlation between the SAXS and infrared data, as mentioned above, the lamellar stack of long period L_2 may be assigned to the ECC morphology. If it is so, the molecular chain length is estimated to be about 7 nm from the long period of L_2 peak. Since POM chain takes a (9/5)

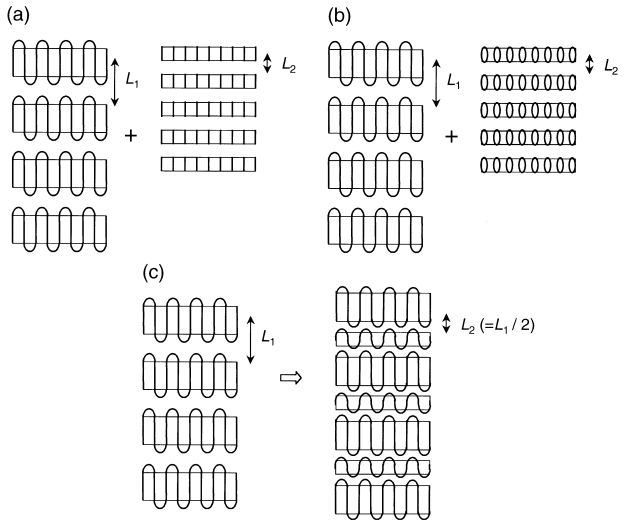

Fig. 12. Illustrated models of stacked lamellar structures. (a) Coexistence of the main lamellar stacking structure and the stacked lamellae of linear low-molecular-weight, (b) coexistence of the main lamellar stacking structure and the stacked lamellae of macrocyclic compounds, and (c) Insertion model of new lamellae in between the already-existing lamellar stacking structure.

helical conformation with repeating period 1.739 nm [42,43], a pitch per one monomeric unit is 1.739/9 = 0.193 nm. Therefore the ECC is speculated to consist of molecular chains of about 36 monomeric units (= 7/0.193 nm). This corresponds to the molecular weight of 1100 g/mol. The averaged molecular weight of the sample used here is 69300 g/mol. The SAXS intensities of the L_1 and L_2 peaks are almost comparable to each other as seen in Fig. 11. Roughly speaking, the intensity is proportional to $(\Delta\rho)^2 \times N$ where $\Delta\rho$ is a difference in electron density between the crystalline and amorphous components forming a lamellar structure and N is a total number of these lamellae. Therefore this POM sample is speculated to consist of bimodal molecular weight distribution of 138,000 and 1100 g/mol with almost equal population [(138,000 + 1,100)/2 = 69,300]. This is quite difficult to imagine for the present POM sample with M_w/M_n 2.3. In other words, it is not reasonable to assign the L_2 peak to such a molecular aggregation structure of fully extended low-molecular-weight component.

Another similar possibility is an existence of low-molecular-weight macrocyclic component of POM. As reported in reference [44], the cationic polymerization reaction of trioxane in the temperature region higher than the melting point gives some amount of macrocyclic compounds as a result of back-biting reaction occurring in a lamella which is crystallized in the reaction bath as the polymerization reaction is proceeded. The length of a ring is estimated to be almost equal to the lamellar thickness, several nm. The total amount of such macrocyclic component is said to be less than 10%. Therefore we have such a possibility that the macrocyclic compounds are crystallized in the cooling process from the melt to give the second peak with ca. 7 nm long period (Fig. 12(b)). But these macrocyclic compounds are reported to show the infrared spectra quite similar to those of FCC [45], inconsistent with the above-mentioned correspondency between the SAXS L_2 and the infrared ECC bands. Besides the relative intensity of the two peaks in the SAXS profile observed at room temperature is also inconsistent with such a fact that macrocyclic compounds contained in POM sample are only several percents. Another important point is that the POM samples Delrin and Tenac, produced by anionic polymerization, do not contain such macrocyclic compounds but they show the similar SAXS profiles with those of the sample used in the present experiment. From all these data, the two SAXS peaks cannot be assumed to come from the separate origins of lamellae (L_1) and macrocyclic compounds (and linear low-molecular-weight compounds) (L_2).

In conclusion the two SAXS peaks are considered to originate from the stacking modes which change at two stages: the L_1 peak due to the stacking structure of original lamellae of long period 14 nm and the L_2 peak due to the lamellar stacking structure of long period 7 nm with the new lamellae inserted in between the originally existing

lamellae as illustrated in model (c) in Fig. 12. How can we understand the intimate correlation between the observation of the SAXS L_2 peak and the infrared ECC bands? We know many examples of such an observation that the two SAXS peaks corresponding to the long periods of L and $L/2$ exchange their relative intensity on the way of crystallization for various kinds of crystalline polymers such as polyethylene [46–49], poly(ethylene terephthalate) [50], poly(aryletheretherketone) [51,52], POM, and also for the blends of different types of polymers [53–57]. It seems more than coincidence to observe such common phenomena for the various types of polymer samples. According to a theory an increase of lamellar thickness in the stacked lamellar structure may cause a change in relative intensity between the 1st-order and 2nd-order SAXS peaks [58], but this model gave us poor SAXS curve fitting and unrealistic structure parameters as will be reported elsewhere. In the present paper we will adopt the model (c) in Fig. 12 and interpret the origin of the L_2 peak and the infrared ECC bands as described in Section 3.4. The detailed and quantitative analysis of the SAXS data of POM sample is now being made on the basis of this insertion model, as will be reported in a separate paper.

3.4. Structural change in the crystallization process

In Fig. 13, various experimental data are plotted against temperature. As for the WAXS data only the changes in the *a*-axial length of the crystal unit cell and the peak position of amorphous halo are presented here, the details of which will be reported in a separate paper. By combining all these data

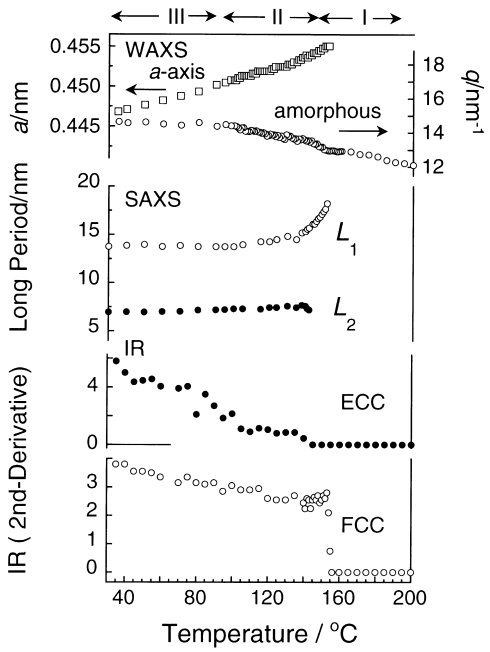

Fig. 13. Temperature dependence of the *a*-axial length of the unit cell, the peak position of the amorphous halo, the long periods of SAXS L_1 and L_2 peaks, and the infrared intensity of ECC and FCC bands (second derivatives estimated for POM sample in the cooling process from the melt).

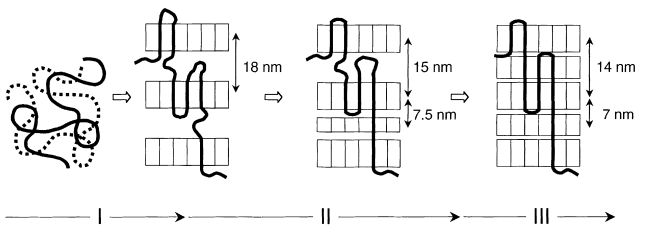

Fig. 14. An illustration of structural evolution in the crystallization process of POM.

obtained by SAXS, WAXS and IR measurements, an image of structural change may be deduced as being illustrated in Fig. 14. Figs. 13 and 14 may be divided into three temperature regions, I, II and III.

Temperature region I. When the sample is cooled from the melt and the temperature reaches the crystallization point, the chain-folded lamellae with the long period of ca. 18 nm are formed. This crystallization occurs steeply in a narrow temperature region. The peak position of the amorphous halo gradually shifts to higher scattering angle and the rate of this shift is slower in the vicinity of crystallization temperature. This observation allows us to speculate that the random coils are more compactly packed with decreasing temperature and change to the crystalline nuclei around the crystallization temperature. The amorphous part which does not participate in the crystallization keeps its random structure during the crystallization, as known from such an observation that the halo peak was not shifted when the crystallization occurred.

Temperature region II. As the temperature decreases from region I, the long period of stacked lamellae is decreased and reaches the almost constant value of ca. 14 nm. Around 140 °C the new lamellae start to appear at a long period of 7 nm (L_2). These new lamellae are considered to locate in between the already existing lamellae, as discussed before (Fig. 12). At the same time, the infrared bands intrinsic of ECC are observed to increase in intensity. As pointed out in the section of infrared spectra, the ECC-like component detected in the crystallization process is considered to be small in size although the R/H ratio is similar to that of a giant whisker. We need to remember again that the infrared ECC bands and the SAXS 7 nm long period were observed in almost the same temperature region. As a possibility a generation of a bundle of taut tie molecules may be speculated, which pass through the several lamellae in a continuous manner and are extended as a whole. Referring to the theoretical curve of frequency shift vs R/H ratio of a cylindrical crystallite [32], the observed frequency position 902 cm^{-1} may correspond to the R/H ratio of ca. 0.1 at most. If the thickness of the original lamella is assumed to be about 5 nm, as will be reported in a separate paper about the quantitative analysis of SAXS data, then the taut tie chain passing through three adjacent lamellae is estimated to have a length of ca. 19 nm. If this length is assumed to be equal to a cylindrical height H, then the radius R is about 1.9 nm. Since the POM helical chain

has a cross sectional area of 0.18 nm^2, the cylindrical crystallite is considered to contain about 60 taut tie chains. According to a computer simulation, the probability to find the tie chains passing through the two adjacent lamellae is about 2% of the whole chains [59]. If the lateral size of a lamella is assumed to be 100 nm at least, then this lamella contains about 56,000 chain stems in detail. The 60 taut tie chains are not impossible at all from these considerations.

Temperature region III. When the temperature approaches 100 °C, the SAXS intensities of the L_1 and L_2 peaks and the infrared intensities of the FCC and ECC bands change their slopes slightly as seen in Fig. 13. The *a*-axial length and the amorphous halo position also change their slopes. These observations may suggest some additional change in the inner structure and/or stacking mode of lamellae in this temperature region. But the detailed discussion cannot be made at the present stage.

4. Conclusions

In this paper, the structural evolution in the cooling process of the molten POM was investigated with various experimental techniques such as DSC, FTIR, WAXS and SAXS. A unique point of this study is to use the infrared spectral technique in order to trace the morphological changes of FCC and ECC and to combine these infrared data with the SAXS and WAXS data. By doing so, the existence of a bundle of taut tie chains is speculated, which continuously pass through the several sheets of lamellae and amorphous region between them. The structural change of POM is complicated: the lamellar stacking structure is changed in the primary (temperature region I) and secondary (temperature region II) crystallization processes as observed in the change of SAXS profiles L_1 and L_2. The lamellar stacking structure formed in the temperature region I becomes tighter in the temperature region II by a generation of second lamellae in between the original lamellae. This is essentially the same phenomenon with those observed for various kinds of polymers. For example, polyethylene shows the lamellar stacking structure of ca. 80 nm long period at the initial stage of crystallization, followed by the generation of new lamellae in between the original lamellae and the long period changes to 40 nm in the next stage [48]. In this case of polyethylene, too, the taut tie chains might be existent. But the infrared spectra of PE are not so sensitive to the shape of crystallite or morphology as the case of POM and cannot tell us explicitly the existence of taut tie chains.

As discussed in the preceding sections the SAXS L_1 and L_2 peaks were combined with the observation of the infrared FCC and ECC bands and the so-called lamellar insertion model was adopted here as the most plausible structure model of POM sample crystallized from the melt. The detailed analysis of the SAXS data will give us more concrete information useful for the model selection, as will be reported in a near future. A possibility of the assignment of the SAXS L_2 peak to the low-molecular-weight compounds and macrocyclic compounds is difficult at present judging from many reasons pointed out in the previous sections.

As easily speculated, the fully extended chains may be produced by applying tensile or shear stress along the chain axis during the crystallization process. Typical example is a development of shish-kebab structure in the fiber spinning process [25]. By measuring the infrared spectra in this process, we might trace more remarkable growth of ECC and FCC regions in the fiber.

Acknowledgements

The authors wish to thank Polyplastics Co. Ltd, Japan for kindly supplying POM sample. They thank also Dr Masatoshi Iguchi (Research Institute for Polymers and Textiles, Tsukuba, Japan) for kindly supplying POM whisker. The authors would like to dedicate this work to the memory of the late Dr Masamichi Kobayashi, emeritus Professor of Osaka University.

References

[1] Cutler DJ, Hendra PJ, Scerri ER, Cudby MEA, Willis HA. Polymer 1979;20:1470.
[2] Franbourg A, Rietsch F. Polym Bull 1990;24:445.
[3] Martin JA, Cruz-Pinto JJC. J Therm Anal 1993;40:621.
[4] Martin JA, Cruz-Pinto JJC, Oliveira MJ. J Therm Anal 1993;40:629.
[5] Cruz-Pinto JJC, Martins JA, Oliveira MJ. Colloid Polym Sci 1994; 272:1.
[6] Plummer CJG, Kausch H-H. Polym Bull (Berlin) 1994;32:117.
[7] Plummer CJG, Kausch H-H. Colloid Polym Sci 1995;273:227.
[8] Plummer CJG, Kausch H-H. Colloid Polym Sci 1995;273:719.
[9] Plummer CJG, Menu P, Cudre-Mauroux N, Kausch H-H. J Appl Polym Sci 1995;55:489.
[10] Phillips R, Manson J-AE. J Polym Sci Polym Phys 1997;B35:875.
[11] Martins JA, Cruz Pinto JJC. Polymer 2002;43:3999.
[12] Geil PH. J Polym Sci 1960;47:65.
[13] Geil PH. J Polym Sci Part C 1966;13:149.
[14] Burmester A, Geil PH. In: Pae RD, Morrow DR, Chen Y, editors. Advances in polymer science and engineering. New York: Plenum Press; 1972. p. 42–100.
[15] Mihailov M, Terlemezyan L. Dokl Bolg Akad Nauk 1975;28:643.
[16] Salaris F, Turturro A, Bianchi U, Martuscelli E, Polymer 1978; 1163
[17] Terlemezyan L, Mihailov M, Schmidt P, Schneider B. Makromol Chem 1978;179:807.
[18] Terlemezyan L, Mihailov M, Schmidt P, Schneider B. Makromol Chem 1978;179:2315.
[19] Terlemezyan L, Mihailov M. Makromol Chem 1978;179:2807.
[20] Schmidt P, Schneider B, Baldrian J, Terlemezyan L, Mihailov M, Ivanova B. Polymer 1987;28:217.
[21] Yeh F, Hsiao BS, Chu B, Sauer BB, Flexman EA. J Polym Sci 1999; B37:3115.
[22] Sauer BB, Hsiao BS, Wang Z-G. Polym Mater Sci Engng 1999;81: 361.
[23] Geil PH. Polymer 2000;41:8983.

[24] Sauer BB, Mclean RS, Londono JD, Hsiao BS. J Macromol Sci Phys 2000;B39:519.
[25] Samon JM, Schultz JM, Hsiao BS, Khot S, Johnson HR. Polymer 2000;42:1547.
[26] Reneker DH, Geil PH. J Appl Phys 1960;31:1916.
[27] Bassett DC. Phil Mag 1964;10:595.
[28] Garber CA, Geil PH. Makromol Chem 1968;113:236.
[29] Iguchi M. Br Polym J 1973;5:195.
[30] Iguchi M, Murase I. J Polym Sci, Polym Phys 1975;13:1461.
[31] Shimomura M, Iguchi M. Polymer 1982;23:509.
[32] Kobayashi M, Sakashita M. J Chem Phys 1992;96:748.
[33] Hoffman JD, Weeks JJ. J Res Nat Bur Std 1962;66A:13.
[34] Jaffe M, Wunderich B, Kolloid ZZ. Polymer 1967;216–217:203.
[35] Iguchi M. Makromol Chem 1976;177:549.
[36] Romankevich OV, Yudin AV. Strukt Mekh Svoistva Vysokomol Soedin Kiev USSR 1976;37–41.
[37] Salaris F, Turturro A, Bianchi U, Martuscelli E. Polymer 1978;19: 1163.
[38] Saavinen PE, Kauppinen JK. In: Chalmer JM, Griffiths PR, editors. Handbook of Vibrational Spectroscopy, vol. 3. Chichester: Wiley; 2002. p. 2185.
[39] Hosemann R, Bagchi SN. Direct analysis of diffraction by matter. Amsterdam: North-Holland; 1962. p. 410.
[40] Crist B. J Polym Sci, Polym Phys 1973;11:635.
[41] Crist B. J Macromol Sci Phys 2000;B39:493.
[42] Tadokoro H, Yasumoto T, Murahashi S, Nitta I. J Polym Sci 1960;44: 266.
[43] Uchida T, Tadokoro H. J Polym Sci A-2 1967;5:63.
[44] Hasegawa M, Yamamoto K, Shiwaku T, Hashimoto T. Macromolecules 1990;23:2629.
[45] Kobayashi M, Sakashita M, Hasegawa M. Macromolecules 1991;24: 4796.
[46] Geil PH. Bull Am Phys Soc 1962;7:206.
[47] Hoffman JD, Weeks JJ. J Chem Phys 1965;42:4301.
[48] Sasaki S, Tashiro K, Kobayashi M, Izumi Y, Kobayashi K. Polymer 1999;40:7125.
[49] Akpalu YA, Amis EJ. J Chem Phys 2000;113:392.
[50] Lee CH, Saito H, Inoue T, Nojima S. Macromolecules 1996;29:7034.
[51] Hsiao BS, Gardner KH, Wu DQ, Chu B. Polymer 1993;34:3986.
[52] Hsiao BS, Gardner KH, Wu DQ, Chu B. Polymer 1993;34:3996.
[53] Song HH, Stein RS, Wu DQ, Ree M, Phillips JC, LeGrand A, Chu B. J Polym Sci, Polym Phys B 1988;21:1180.
[54] Song HH, Wu DQ, Chu B, Satkowski M, Ree M, Stein RS, Phillips JC. Macromolecules 1990;23:2380.
[55] Li Y, Jungnickel B-J. Polymer 1993;34:9.
[56] Dreezen G, Mischenko N, Koch MHJ, Reynaers H, Groeninckx. Macromolecules 1999;32:4015.
[57] Yeh F, Hsiao BS, Chu B, Sauer BB, Flexman EA. J Polym Sci, Polym Phys B 1999;37:3115.
[58] Schultz JM, Lin JS, Hendricks RW. J Appl Cryst 1978;11:551
[59] Balijepalli S, Rutledge GC. Comp Theo Polym Sci 2000;10:103.